J|A|C|S
ARTICLES

Published on Web 09/03/2008

Wired-Enzyme Core−Shell Au Nanoparticle Biosensor

P. Scodeller,[†] V. Flexer,[†] R. Szamocki,[†] E. J. Calvo,*[,†] N. Tognalli,[‡] H. Troiani,[‡] and A. Fainstein[‡]

INQUIMAE, Facultad de Ciencias Exactas y Naturales, Universidad de Buenos Aires, Pabellón 2, Ciudad Universitaria, 1428 Buenos Aires, Argentina, and Centro Atomico Bariloche and Instituto Balseiro, Comision Nacional de Energia Atomica, 8400 S.C. de Bariloche, Argentina

Received March 30, 2008; E-mail: calvo@qi.fcen.uba.ar

Abstract: We report a fully integrated core−shell nanoparticle system responsive to glucose. The system is comprised of self-assembled glucose oxidase and an osmium molecular wire on core−shell Au nanoparticles. Characterization of the functional nanoparticles by spectroscopy, quartz crystal microbalance and electrochemical techniques has shown that the catalytically active shell has a structure as designed and all components are active in the self-assembled multilayer shell. Furthermore, amperometric reagentless detection of glucose and contactless photonic biosensing by the Os(II) resonant Raman signal have been demonstrated. The enzymatic reduction of FAD by glucose and further reduction of the Raman silent Os(III) by $FADH_2$ yields a characteristic enzyme−substrate calibration curve in the millimolar range. Furthermore, coupling of electronic resonant Raman of the osmium complex with the SERS amplification by Au NPs plasmon resonance has been demonstrated which leads to an extra enhancement of the biosensor signal. We present a proof of concept extending the work done with planar surfaces to core−shell NPs as an advance in the design of glucose-responsive chemistry detected by SERS-like methods.

Introduction

The emerging field of nanobiotechnology offers new exciting possibilities with nanoparticles applied to the analysis of biomolecules.[1,2] The ability to sense biological molecules in vitro or in vivo with high amplification while reducing the sample size and with high selectivity can be accomplished because of the distinctive electronic, optical, and magnetic properties in the nanoscale. Nanoparticles have been reported in different biosensing devices using different transduction methods such as colorimetric,[3] fluorescent,[4] electrochemical,[5] surface plasmon resonance,[6] magnetic,[7] and in particular surface-enhanced Raman scattering.[2,8−11]

Core−shell colloidal particles with layer-by-layer (LbL) assembled polyelectrolytes multilayers have been introduced by Caruso and co-workers[12−15] following the sequential adsorption method developed by Decher for flat surfaces.[16] One of the most interesting applications is the use of proteins[17] and enzymes[18] on metallic colloidal particles and hollow microcapsules.[18−23] These systems can be employed for the release of molecules in living cells[24] and biosensing applications.[21]

Reagentless integrated supramolecular enzyme amperometric electrodes have attracted considerable attention.[25−28] In these biosensors, a sequence of electron hopping events in the redox

[†] Universidad de Buenos Aires.
[‡] Comision Nacional de Energia Atomica.

(1) Penn, S.; He, L.; Natan, M. *Curr. Opin. Chem. Biol.* **2003**, *7*, 609–615.
(2) Doering, W. E.; Piotti, M. E.; Natan, M. J. *Adv. Mater.* **2007**, *19*, 3100–3108.
(3) Elghanian, R.; Storhoff, J. J.; Mucic, R. C.; Letsinger, R. L.; Mirkin, C. A. *Science* **1997**, *277*, 1078–1081.
(4) Maxwell, D. J.; Taylor, J. R.; Nie, S. M. *J. Am. Chem. Soc.* **2002**, *124*, 9606–9612.
(5) Willner, I.; Willner, B.; Katz, E. *Bioelectrochemistry* **2007**, *70*, 2–11.
(6) He, L; Musick, M. D.; Nicewarner, S. R.; Salinas, F. G.; Benkovic, S. J.; Natan, M. J.; Keating, C. D. *J. Am. Chem. Soc.* **2000**, *122*, 9071–9077.
(7) Perez, J. M.; Simeone, F. J.; Tsourkas, A.; Josephson, L.; Weissleder, R. *Nano Lett.* **2004**, *4*, 119–122.
(8) Qian, X. M.; Peng, X. H.; Ansari, D. O.; Yin-Goen, Q.; Chen, G. Z.; Shin, D. M.; Yang, L.; Young, A. N.; Wang, M. D.; Nie, S. *Nat. Biotechnol.* **2008**, *26*, 83–90.
(9) Willets, K. A.; Van Duyne, R. P. *Annu. Rev. Phys. Chem.* **2007**, *58*, 267–297.
(10) Qian, X.; Peng, X. H.; Ansari, D. O.; Yin-Goen, Q.; Chen, G. Z.; Shin, D. M.; Yang, L.; Young, A. N.; Wang, M. D.; Nie, S. M. *Nat. Biotechnol.* **2007**,
(11) Qian, X. M.; Peng, X. H.; Ansari, D. O.; Yin-Goen, Q.; Chen, G. Z.; Shin, D. M.; Yang, L.; Young, A. N.; Wang, M. D.; Nie, S. M. *Nat. Biotechnol.* **2008**, *26*, 83–90.
(12) Caruso, F. *Adv. Mater.* **2001**, *13*, 11.
(13) Caruso, F.; Caruso, R. A.; Mohwald, H. *Science* **1998**, *282*, 1111–1114.
(14) Gittins, D. I.; Caruso, F. *Adv. Mater.* **2000**, *12*, 1947.
(15) Gittins, D. I.; Caruso, F. *J. Phys. Chem. B* **2001**, *105*, 6846–6852.
(16) Decher, G. *Science* **1997**, *277*, 1232–1237.
(17) Caruso, F.; Mohwald, H. *J. Am. Chem. Soc.* **1999**, *121*, 6039–6046.
(18) Caruso, F.; Schuler, C. *Langmuir* **2000**, *16*, 9595–9603.
(19) Yu, A. M.; Liang, Z. J.; Caruso, F. *Chem. Mater.* **2005**, *17*, 171–175.
(20) Wang, Y. J.; Caruso, F. *Chem. Commun.* **2004**, 1528–1529.
(21) Yu, A. M.; Caruso, F. *Anal. Chem.* **2003**, *75*, 3031–3037.
(22) Jin, W.; Shi, X. Y.; Caruso, F. *J. Am. Chem. Soc.* **2001**, *123*, 8121–8122.
(23) Schuler, C.; Caruso, F. *Macromol. Rapid Commun.* **2000**, *21*, 750–753.
(24) Skirtach, A. G.; Javier, A. M.; Kreft, O.; Kohler, K.; Alberola, A. P.; Mohwald, H.; Parak, W. J.; Sukhorukov, G. B. *Angew. Chem., Int. Ed.* **2006**, *45*, 4612–4617.
(25) Calvo, E. J.; Danilowicz, C. B.; Wolosiuk, A. *Phys. Chem. Chem. Phys.* **2005**, *7*, 1800–1806.
(26) Calvo, E. J.; Wolosiuk, A. *Chemphyschem* **2005**, *6*, 43–47.
(27) Calvo, E. J.; Wolosiuk, A. *Chemphyschem* **2004**, *5*, 235–239.
(28) Calvo, E. J.; Danilowicz, C.; Wolosiuk, A. *J. Am. Chem. Soc.* **2002**, *124*, 2452–2453.

 10.1021/ja802318f CCC: $40.75

polymer follows electron transfer between adequately positioned redox centers and $FADH_2$ prosthetic group of glucose oxidase (GO*x*) or other flavoenzymes[29] to yield an electrical current in the external circuit. Adam Heller introduced a two-component epoxy technique combining GO*x* and other oxidases with a polycationic redox mediator cross-linked with a bifunctional reagent to yield a self-contained biosensor.[30]

The step-by-step electrostatic adsorption of charged molecules in solution onto a surface bearing opposite charge, introduced by Gero Decher,[16] provides a fine control at the molecular level. With this method the adsorption of polymers and biomolecules can be restricted to a monolayer by charge self-regulation in each immersion step. In 1997 Hodak et al.[31] showed for the first time effective electrical wiring of glucose oxidase by a redox polymer self-assembled layer-by-layer on a thiolated gold surface. Alternate layers of glucose oxidase and a ferrocene redox polymer were assembled sequentially. The redox charge and the amount of "wired enzyme" increased with the number of deposited layers, but only a small fraction of the total active enzyme was found to be efficiently "electrically wired" by the ferrocene polymer. A more stable osmium pyridine−bipyridine complex tethered to the linear polymer poly-(allylamine), (PAH-Os) and the anionic enzyme glucose oxidase, GO*x*, deposited stepwise in similar alternate polymer enzyme multilayers was studied by quartz crystal microbalance (QCM), atomic force microscopy (AFM), and electrocatalysis.[32,33] The structure and dynamics of the self-assembled redox active polyelectrolyte and enzyme multilayers were investigated by quartz crystal microbalance (QCM),[28,34] ellipsometry,[28,34] FTIR,[35] and resonant Raman spectroscopy.[36] A linear increase in the film thickness, enzyme loading, and catalytic current with the number of dipping cycles has been found.

In this article we present a proof of concept extending the work done with planar surfaces to core−shell NPs with new aspects as the contactless interrogation by resonant Raman spectroscopy which can discriminate the Os(II) redox state that reports the concentration of glucose in the sample. There are several novel and important aspects in this manuscript: First, a new design of an integrated chemical system responsive to glucose; second, each core−shell nanoparticle is loaded with all active components to recognize glucose and report by resonant Raman signal; and third, each NP is capable of producing a SERS effect besides the electronic resonant Raman independently of the use of enhancing surface platforms.

Experimental Details

For spectrophotometric analysis, quartz cuvetes (Hellma SUPRASIL, path length 10 mm) and a HP1603 double beam spectrophotometer were used with Eppendorf 5415D centrifuge and 1.5 mL disposable Eppendorf tubes. All reagents were purchased from Sigma-Aldrich and used without further purification. Water was deionized and filtered using a Millipore water purification system (18 MΩ).

Synthesis of Gold Nanoparticles. Gold nanoparticles were synthetized by a modification of the Turkevich method: In brief, 4.5 mg of tetrachloroauric acid ($HAuCl_4$) was dissolved in 45 mL of MilliQ water, and 10 mL of this solution was brought to boil in a round-bottom flask under stirring. A 1.6 mL portion of a 1% sodium citrate solution and 10 μL of 4.2 mg MPS (mercapto propane sulfonate)/100 μL water was added simultaneously to the solution using a stirrer. The solution turned red after 5 min, and the intensity of the color increased with time. Boiling was maintained for 20 min after which the heat was removed and stirring was continued for 15 min. The nanoparticles were then filtered through Whatman No.1 filter paper to remove impurities. Then, 8 mL of the nanoparticle suspension were centrifuged in 1.5 mL Eppendorf tubes at 7000 rpm (4.500*g*) during 45 min to remove excess thiol; the supernatant was removed, and the remaining NPs were redispersed in 4 mL of water.

Synthesis of Core−Shell Nanoparticles. Poly(allylamine), PAH, derivatized with an osmium pyridine−bipyridine complex covalently attached to the polymer backbone, PAH-Os was employed as redox polyelectrolyte. Repetitive alternate adsorption of PAH-Os and GO*x* on the MPS thiolated Au NP was performed in the following way: 4 mL of nanoparticle suspension (6.8×10^{-10} M) was added to 4 mL of 4.4×10^{-4} M PAH-Os solution of pH 8.75 under stirring at room temperature; this solution was left for 20 min, and then the nanoparticles were washed three times to remove excess PAH-Os (45 min at 7000 rpm, 4.500*g*, each washing cycle) and brought to a final volume of 4 mL. This 4 mL was added to 4 mL of 10 mg GO*x* in 20 mL of TRIS buffer of pH = 8, 20 mM under stirring, and at room temperature. The solution was left for 1 h, after which the nanoparticles were washed to remove excess GO*x* by three washing cycles during 45 min at 7000 rpm (4.500*g*) each. These deposition steps were repeated until the desired number of polymer and enzyme layers were deposited.

Oxidation of Os(II) Nanoparticles. The Os(II) bipyridine−pyridine complex cannot be oxidized directly by molecular oxygen or hydrogen peroxide even in the presence of Au nanoparticles (see Supporting Information). Therefore, 20 μL of 1 μg/mL soybean peroxidase was added to 500 μL of nanoparticle solution (3×10^{11} particles/mL) and incubated for 5 min. Then, 25 μL of a 3 μM H_2O_2 solution was added, and the solution was incubated for 15 min. Three 45 min washing cycles at 7000 rpm (4.500*g*) were performed to separate the nanoparticles which were then redispersed in a final volume of 30 μL. The oxidation of PAH-Os(II) with H_2O_2 catalyzed by soybean peroxidase (SBP) and further reduction with glucose has been followed by UV−visible spectroscopy. Figure 1 in the Supporting Information shows the process of Os(II) oxidation in PAH-Os solution by hydrogen peroxide catalyzed by soybean peroxidase (SBP) and further recovery of the Os(II) by reduction with glucose in the presence of GO*x*. The broad absorbance band in the 450−550 nm range due to the metal-to-ligand charge transfer (MLCT) transition characteristic of the Os(II) demonstrates a 20% recovery of the Os(II). The MLCT band could not be followed in the presence of core−shell NPs because of the stronger absorption of the Au plasmon band at 530 nm.

Microscopy. A Philips CM 200 TEM transmission microscope equipped with an ultrathin objective lens was used and the acceleration voltage was 200 keV. For TEM observations the core−shell Au nanoparticles were deposited on ultrathin commercial carbon support films deposited on Cu grids. The thickness of the carbon film was approximately 4 nm.

For AFM experiments, a multimode NanoScope IIIa SPM (Digital Instruments-Veeco) and AFM images were recorded in tapping mode in air, (TM-AFM) with a piezoelectric J scanner with lateral scan range of 150 μm using Si_3N_4 cantilevers with an elastic constant of 0.32 N/m (Nano Devices, Veeco).

(29) Vilkanauskyte, A.; Erichsen, T.; Marcinkeviciene, L.; Laurinavicius, V.; Schuhmann, W. *Biosens. Bioelectron.* **2002**, *17*, 1025–1031.
(30) Heller, A. *J. Phys. Chem.* **1992**, *96*, 3579–3587.
(31) Hodak, J.; Etchenique, R.; Calvo, E. J.; Singhal, K.; Bartlett, P. N. *Langmuir* **1997**, *13*, 2708–2716.
(32) Calvo, E. J.; Etchenique, R.; Pietrasanta, L.; Wolosiuk, A.; Danilowicz, C. *Anal. Chem.* **2001**, *73*, 1161–1168.
(33) Calvo, E. J.; Battaglini, F.; Danilowicz, C.; Wolosiuk, A.; Otero, M. *Faraday Discuss.* **2000**, 47–65.
(34) Flexer, V.; Forzani, E. S.; Calvo, E. J. *Anal. Chem.* **2006**, *78*, 399–407.
(35) Bonazzola, C.; Calvo, E. J.; Nart, F. C. *Langmuir* **2003**, *19*, 5279–5286.
(36) Tognalli, N.; Fainstein, A.; Bonazzola, C.; Calvo, E. J. *J. Chem. Phys.* **2004**, *120*, 1905–1911.

Quartz Crystal Microbalance Measurements. The quartz crystal resonator at 10 MHz was used as a quartz crystal microbalance with a complex voltage divider to measure the resonant frequency and both of the components of the quartz crystal Butterworth−Van Dyke equivalent circuit. AT-cut 10-MHz quartz crystals (International Crystal Manufacturing Co. Inc., Oklahoma City, OK; Catalog No. 31210) 14-mm diameter and 0.168 mm thick, with an active area of 0.196 cm^2 with a roughness factor of 1.2 measured by AFM, were employed. The crystals were mounted in the cells by means of Viton O-ring seals, with only one face in contact with the electrolyte; this electrode was a common ground to both the ac and dc circuits (see ref 32 for details). A 40 μL portion of a suspension of 3.2×10^{-9} M of Au core−shell NPs dispersion was added under stirring to 1 mL of water above the Au-coated quartz crystal. Measurement of the R parameter of the BVD equivalent circuit, which measures the viscoelastic losses of the shear wave at the interface, indicated that the system behaves as acoustically thin and therefore the changes in the real component of the quartz crystal impedance or frequency shift can be taken as changes of mass on the crystal.

Electrochemical Experiments. Gold electrodes used for electrochemical experiments were thoroughly cleaned by inmersion in a hot 1:1 nitric/sulfuric acid for several hours. Clean electrodes were further rinsed with Milli-Q water. The gold surface was modified with sulfonate groups by immersion in a freshly prepared 20 mM MPS solution in 10 mM H_2SO_4 for 30 min followed by rinsing with Milli-Q water. For nanoparticle adsorption, 40 μL of 3.2×10^{-9} M of the nanoparticle dispersion were placed on the electrode surface, the cell was sealed to prevent water evaporation, and this was left overnight at 4 °C. The nanoparticle solution was removed, and the electrode was then rinsed with copious Milli-Q water. A standard three-electrode electrochemical cell was employed with an operational amplifier potentiostat (TEQ-Argentina). For reference electrode Ag/AgCl 3 M was employed and all electrode potentials are referred to it; a platinum gauze auxiliary electrode of large area was employed. All electrochemical experiments were carried out in 4 mL of phosphate buffer solutions 0.1 M, pH = 7, 0.1 M NaCl, at room temperature.

After performing cyclic voltammetry in glucose free solutions, 400 μL of 1 M mutarotated glucose were added to the same cell to a final concentration of 0.1 M, and a low scan (1 mV/s) voltammetry was performed.

Resonant Raman Scattering. The resonant Raman scattering experiments were performed using a Jobin-Yvon T64000 triple spectrometer operating in subtractive mode and equipped with a liquid N_2 cooled charge coupled device (CCD). The excitation was done between 1.916 eV (~647 nm) and 2.707 eV (~458 nm) using the 17 lines of an Ar−Kr ion laser, with 10 mW power focused on a ~100 μm diameter spot.

Results and Discussion

A. Fabrication and Characterization. The self-assembly process of the enzyme-redox polymer multilayers on gold nanoparticles was followed by UV−visible spectroscopy. The spectra of Au NPs were recorded after each adsorption and washing step by placing 500 μL of the solutions in a 1 cm quartz microcuvette (VWR). The spectra were recorded in the 200−800 nm interval using MilliQ (Millipore) water as baseline.

Figure 1 depicts a typical series of these spectra with a Au plasmon band at 528 nm for the as prepared thiol capped Au NPs and slightly red-shifted for the rest of the core−shell NPs. Since the extinction coefficient for Au NP is very large at plasmon resonance, ca. $\varepsilon = 10^9$ M^{-1} cm^{-1},[37,38] while the extinction coefficient for the metal-to-ligand charge transfer (MLCT) transition in the osmium pyridil−bipyridine complex

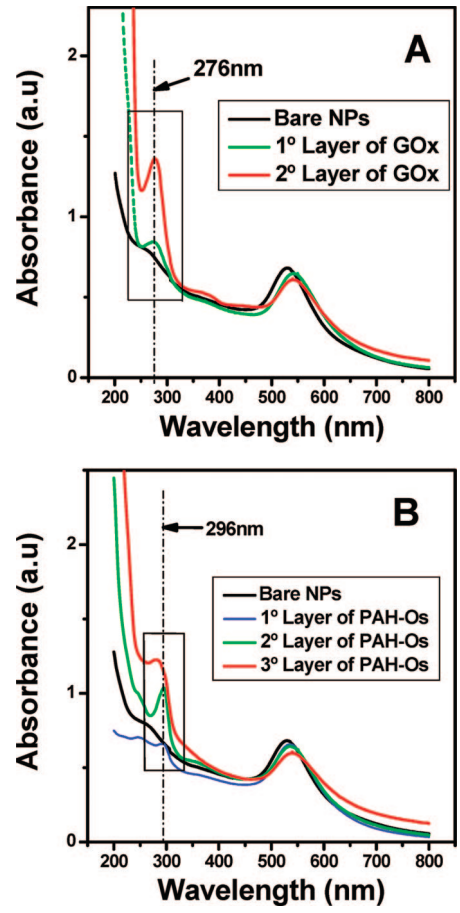

Figure 1. UV−visible absorption spectra of Au NPs suspension ($\varepsilon = 10^9$ $M^{-1}cm^{-1}$, $A = 0.6813$; $C = 6.8 \times 10^{-10}$ M) after the successive additions of PAH-Os layers ($\varepsilon_{max} = 8.1 \times 10^3$ M^{-1} cm^{-1} at 467 nm) and GO*x* solutions, respectively: (A) succesive layers capped with GO*x*; (B) succesive layers capped with PAH-Os.

is much less, ca. $\varepsilon = 8 \times 10^3$ M^{-1} cm^{-1},[34] only the plasmon band is apparent in the visible range at ca. 500 nm. A second band in the UV at 296 nm characteristic of the osmium complex with $\varepsilon = 4 \times 10^4$ M^{-1} cm^{-1} (see Supporting Information) has been employed to determine the amount of osmium polymer self-assembled in each adsorption step while the absorption of GO*x* was followed at 276 nm. For clarity in Figure 1 the sequential adsorption of GO*x* and PAH-Os separately are shown in Figure 1A and 1B, respectively.

While there is a small but consistent change in the position of the plasmon absorption band toward higher wavelength, there is no net red shift due to particle aggregation in solution.[39−41] Changes in local dielectric constant environment upon modification of the Au nanoparticles with polyelectrolyte and enzyme could explain the small shift (ca. 5−10 nm) and line broadening of the plasmon band.[42,43]

Examination of the absorption spectra shows the increase of intensity of the peaks centered at 276 nm (Figure 1A) and 296

(37) Link, S.; El-Sayed, M. A. *J. Phys. Chem. B* **1999**, *103*, 8410–8426.
(38) Mulvaney, P. *Langmuir* **1996**, *12*, 788–800.
(39) Bellino, M. G.; Calvo, E. J.; Gordillo, G. *Phys. Chem. Chem. Phys.* **2004**, *6*, 424–428.
(40) Weisbecker, C. S.; Merritt, M. V.; Whitesides, G. M. *Langmuir* **1996**, *12*, 3763.
(41) Sendroiu, I. E.; Mertens, S. F. L.; Schiffrin, D. J. *Phys. Chem. Chem. Phys.* **2006**, *8*, 1430–1436.
(42) Mulvaney, P. *Langmuir* **1996**, *12*, 788–800.
(43) Jensen, P. S.; Chi, Q.; Grumsen, F. B.; Abad, J. M.; Horsewell, A.; Schiffrin, D. J.; Ulstrup, J. *J. Phys. Chem. C* **2007**, *111*, 6124–6132.

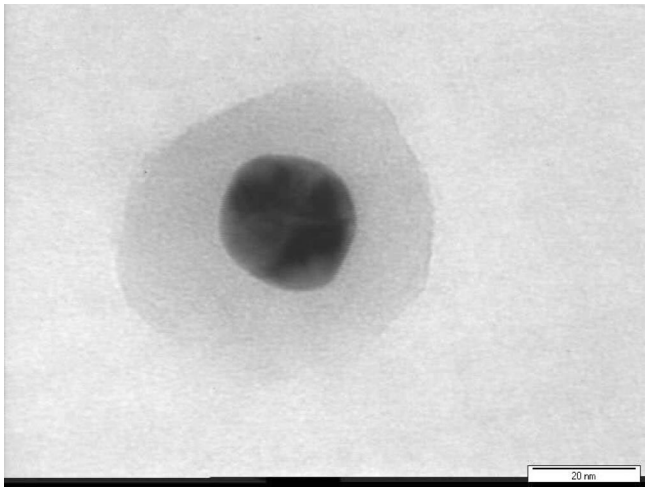

Figure 2. Typical TEM micrograph of a core−shell Au nanoparticle Au/(PAH-Os)$_4$(GOx)$_3$.

nm (Figure 1B), respectively, which demonstrates the deposition of glucose oxidase and the osmium complex derivatized poly(allylamine) in each sequential adsorption step.

Transmission electron microscopy (TEM) of the resulting core−shell Au NPs in Figure 2 shows the thickness of the glucose oxidase-redox polyelectrolyte shell around the Au core with a distinct contrast for the gold and the osmium containing soft matter. From the images of many particles (see Supporting Information) it is possible to observe that the Au core dimension is 20 nm and the polyelectrolyte-enzyme shell is clearly seen with a thickness of 20 nm approximately in the dry state. High resolution transmission electron microscopy (HRTEM) observations also confirmed that the Au cores are crystalline.

The thickness of the multilayer shell for three enzyme and four polyelectrolyte layers was found to be 19 nm, in good agreement with previous ellipsometric studies of the same system on flat Au surfaces under similar conditions while self-assembly from solutions of lower pH results in thinner films.[34] The core−shell nanoparticles in Figure 2 are similar to poly(allylamine)-poly(styrene sulfonate) core−shell NPs reported by Decher[44] but exhibit a thicker polyelectrolyte shell due to the pH dependent charge density of PAH-Os[34] and the enzyme size.

The functional Au-core enzyme shell nanoparticles with positive charge in the topmost poly-(allylamine) layer were deposited on Au substrates thiolated with negatively charged mercapto propane sulfonate (MPS) and the adsorption process was followed by quartz crystal microbalance (QCM). Figure 3 shows the mass uptake during the NPs adsorption with a maximum of 1.6 μg cm^{-2}, which corresponds to 2×10^{10} NPs per square centimeter on the basis of particle size and gold density.

Atomic force microscopy examination of this surface shows a random distribution of nonaggregated spherical nanoparticles on the thiolated Au surface, but no evidence of the shell structure can be seen with this technique (see Figure 4b). For comparison an AFM control image of MPS-thiolated Au surface is shown in Figure 4a. A statistical analysis of 2400 NPs in a 5×5 μm^2 field gave an average of 0.96×10^{10} NPs per square centimeter in good agreement with the gravimetric evidence. A height size

(44) Schneider, G.; Decher, G. *Nano Lett.* **2004**, *4*, 1833–1839.

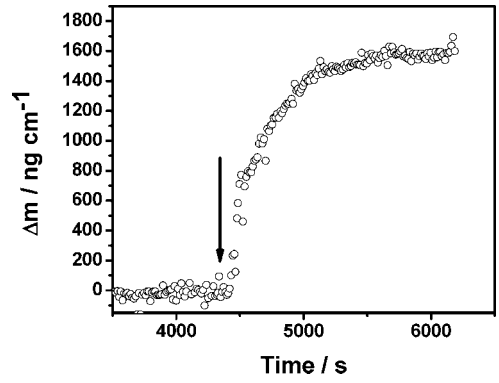

Figure 3. Quartz crystal microbalance gravimetry for the uptake of core−shell Au/PAH nanoparticles from a 5×10^{-9} M dispersion on a MPS-thiolated Au surface.

distribution analysis and line profiles (see Figure 4c, d) yields NPs of 18.3 ± 4.6 nm in diameter.

Confirmation of both redox and enzyme activity of the functional Au core enzyme−redox polymer shell nanoparticles was obtained electrochemically. Cyclic voltammetry in Figure 5A shows peaks characteristic of redox species confined to the electrode surface for the oxidation−reduction of the osmium complex in the NP shells positioned at suitable tunneling distance from the gold electrode. The half-wave potential $E_{1/2}$ = 0.30 V and a peak full width at half-height (fwhh) 200 mV are in good agreement with previous studies of this redox polymer[25,28,32] and confirm the presence of the osmium complexes at the NPs surface. Furthermore, integration of the area under oxidation and reduction peaks yields a redox charge of 0.9 μC cm^{-2} which corresponds to 10^{-11} mol cm^{-2} for the one electron osmium redox center, much less than the osmium complex carried by the 10^{10} nanoparticles in 1 cm^2 of electrode surface. For an electron hopping diffusion coefficient of 10^{-9} cm^2 s^{-1},[26] the osmium centers far from the electrode surface are inaccessible in the experimental time scale.

By addition of glucose to the electrolyte we have verified the activity of wired enzyme by the redox polyelectrolye, PAH-Os, in the NPs shell. Figure 5B depicts the current−potential curves at slow scan rate in the absence and in the presence of 0.1 M glucose in solution, respectively. An increase of the current in the presence of glucose is clearly seen and subtraction of the background current in the absence of glucose is shown in Figure 5C, which depicts a clear redox enzyme catalytic wave tuned at the redox potential of the osmium complex which acts as electron shuttle between the Au electrode or Au nanoparticles and the prosthetic $FADH_2$ group in the enzyme immobilized within the shell multilayer.[28]

So far we have shown that the catalytically active core shell NPs have a structure as designed and all the components are active in the self-assembled multilayer shell. Thus, the NPs adsorbed on an electrode surface can yield an amperometric enzyme biosensor signal. We will next demonstrate the capability of this system as a glucose nano biosensor when interrogated by photons. For this we have used Resonant Raman spectroscopy to detect the redox state of the osmium in the self-assembled multilayer shell which should report on the concentration of glucose in the solution in contact with the nanoparticles.

B. Raman Spectroscopic Interrogation of Os(II). In previous studies[36] we have reported that the Os(II) pyridine−bipyridine complex exhibits resonant Raman effect when excited in the metal (Os)-to-ligand charge transfer (MLCT) absorption band

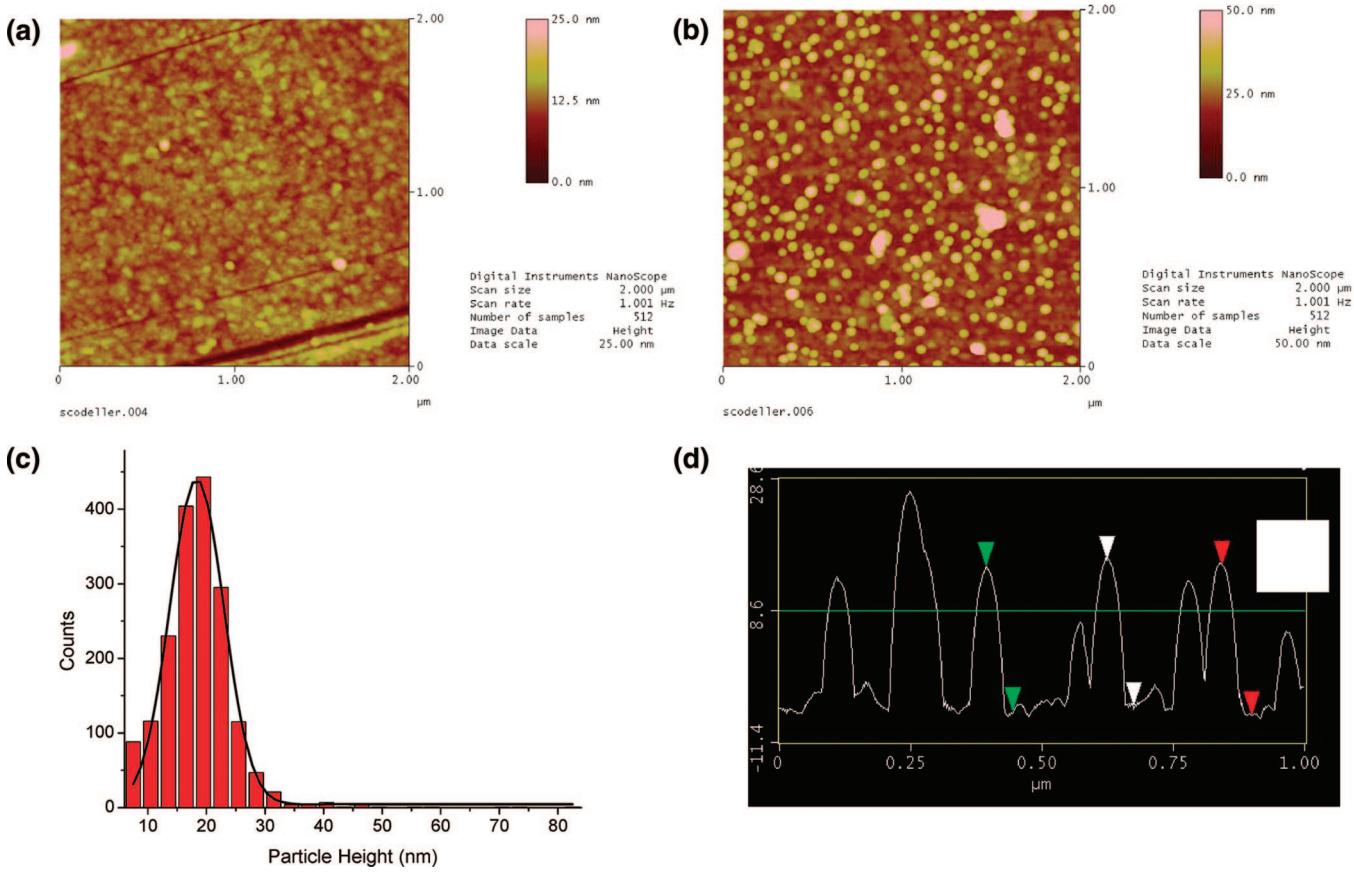

Figure 4. (a) AFM control image of MPS-thiolated Au surface on the same quartz crystal of Figure 3 before NP treatment. (b) AFM image of core−shell Au/PAH nanoparticles adsorbed onto a MPS-thiolated Au surface on the same quartz crystal of Figure 3. (c) NPs height histogram. (d) Line profile in panel b.

(514.5 nm). The characteristic modes of pyridine and bipyridines (670 cm^{-1}, related to a pyridine bending mode, and between 1325 and 1606 cm^{-1} related to pyridine stretching vibrations) and Os−N metal−ligand mode (383 cm^{-1}) are clearly seen in Figure 6a (as grown). Scheme 1 shows the schematic representation of the osmium pyridine−bipyridine complex and a simplified molecular orbital diagram for the Os(II) and Os(III) oxidation states. Note that the MLCT transition for Os(II) lies in the visible range, while for the oxidized Os(III) state it shifts to higher energies (i.e., $\lambda < 300$ nm). Therefore, we expect a resonant Raman effect with excitation at ca. 500 nm for the Os(II), while at this laser line no resonant scattering is expected for the oxidized osmium species, Os(III).[36] This is confirmed since, upon oxidation in the Os(III) state, quenching of the Raman resonance is observed due to the shift of the absorption band into the ultraviolet as depicted in Scheme 1. It is this dependence of the Raman intensity on the complex oxidation state that will be used as an optical probe of glucose concentration as depicted in Scheme 2.

The core−shell sensors described here are based on the Os complex with Raman properties as described above but, in addition, are built on top of a Au NP with the plasmonic response displayed in Figure 1. Thus, a plasmon-induced surface enhancement of the Raman signal (SERS) is expected, which should add to the described electronic resonance to provide a particularly sensitive Raman probe. To evidence the presence of SERS amplification we present next a comparison of the resonant Raman response of the PAH-Os complex in a layer-by-layer grown supramolecular structure of $(PAH\text{-}Os)_4/PVS)_3$ grown on a glass substrate (i.e., without SERS effect), with that of the core−shell nanosensor.

Figure 7a shows the Raman intensity of the 1550 cm^{-1} peak for the osmium complex bipyridine mode in PAH-Os as a function of the laser excitation energy. For the pure electronic resonance of PAH-Os we identify two intensity maxima related to the incoming and outgoing electronic Raman resonances at 515 and 482 nm, respectively.[36,45] The first peak, at 515 nm, is due to the energy tuning between the incident photon and the osmium pyridine−bipyridine complex MCTL transition. The second peak, which depends on the analyzed vibrational mode, arises from the tuning of the scattered photon with the MCTL transition. Thus, the Raman signal has maxima at energies around the PAH-Os absorption peak and decays for excitation at wavelengths above 550 nm as the MCTL absorption broadband fades away (Figure 7b).

The Raman scattering for the osmium complex in the multilayer polymer, PAH-Os, adsorbed in the core−shell Au nanoparticles shows a quite distinct profile as a function of laser excitation energy (labeled NP+PAH-Os) (see Figure 7a). The resonance maximum shifts to lower energies (∼530 nm) and a much broader featureless response is observed. In fact, when comparing with the NP absorption reproduced in Figure 7b it is quite clear that the maximum absorbance due to the Au plasmon at 530 results in a maximum Raman scattering peak associated to the SERS effect. It is furthermore noteworthy that,

(45) Tognalli, N.; Fainstein, A.; Calvo, E.; Bonazzola, C.; Pietrasanta, L.; Campoy-Quiles, M.; Etchegoin, P. *J. Chem. Phys.* **2005**, *123*.

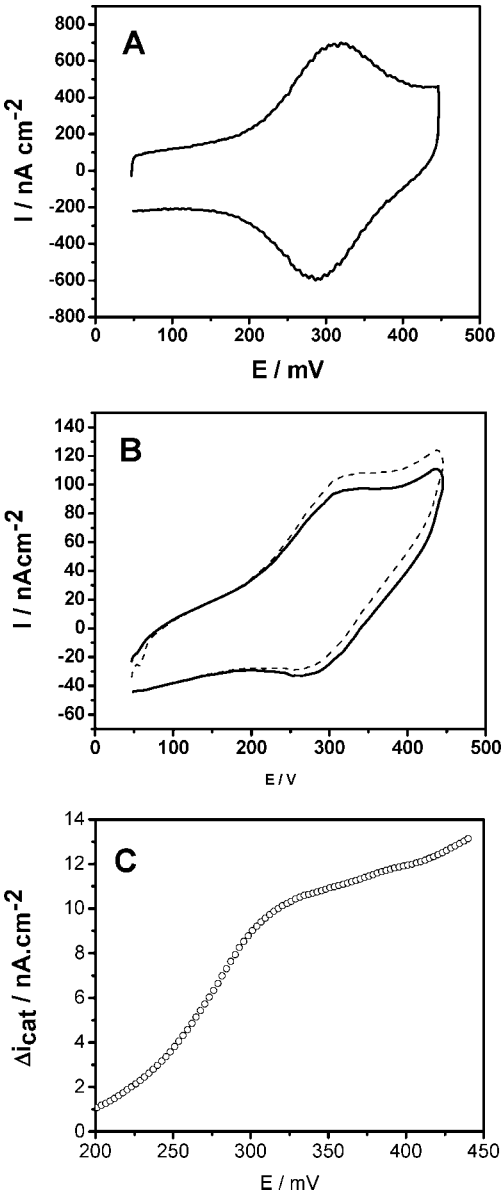

Figure 5. (A) Cyclic voltammetry of core−shell Au/(PAH-Os)$_3$(GOx)$_2$ nanoparticles adsorbed on an MPS-thiolated Au at 50 mV s^{-1} in glucose free 0.1 M phosphate buffer of pH 7 in 0.1 M NaCl. Integration of the curve yields an average of 0.9 ± 0.1 μC cm^{-2} of osmium complex. (B) Cyclic voltammetry at 1 mV s^{-1} in the absence of glucose (continuous line) and after the addition of glucose to a final concentration of 0.1 M (dotted line) in the same electrolyte as in panel A. (C) Differential catalytic current vs potential plot for data in panel B after subtraction of current baseline in the absence of glucose.

unlike the electronic resonant Raman scattering of the PAH-Os alone, on core−shell NPs the intensity of the bipyridine Raman scattering extends over the 550−650 nm region following the Au plasmon absorption profile. We note that this behavior is almost identical to that observed for the SERS response of a (PAH-Os)(Au NP)(PAH-Os) structure containing a monolayer of isolated 18 nm Au nanoparticles sandwiched between two layers of the Os-complex.[45]

Our strategy to sense glucose (see Scheme 2) has been to recover the resonant Raman signal due to the Os(II) complex in the NPs shell via the enzymatic reduction of the Raman silent Os(III) complex in the presence of glucose and catalyzed by glucose oxidase in the NPs shell. In the Supporting Information we show that Os(II) cannot be directly oxidized by reaction

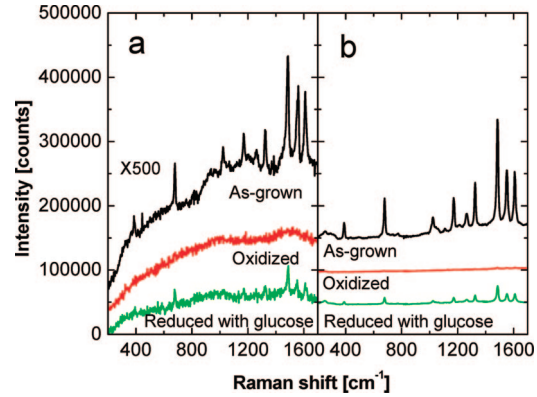

Figure 6. (a) Resonant Raman spectra of Au core (PAH-Os)$_4$(GOx)$_3$ shell nanoparticles deposited on an atomically flat Au substrate for (i) as grown Os(II), (ii) oxidized Os(III), and (iii) after addition of glucose solution (200 mM). The excitation was with 514.5 nm, 10 mW, and 10 s acquisition time. (b) The same as panel a but with the core−shell NPs deposited on 700 nm Ag cavities. Note the ×500 enhancement of the signals but otherwise the same relation between spectra from samples reduced, oxidized, and in contact with glucose.

Scheme 1. Schematic Representation of the PAH-Os Complex Used in the Self-Assembled Multilayer Shells and Simplified Molecular Orbital Diagram for Os(II)/Os(III) and Bipyridine Ligands in the [Os(bpy)$_2$PyCl]$_2^+$ Complex. The Corresponding MLCT Transitions in both Os States Are Represented by Arrows

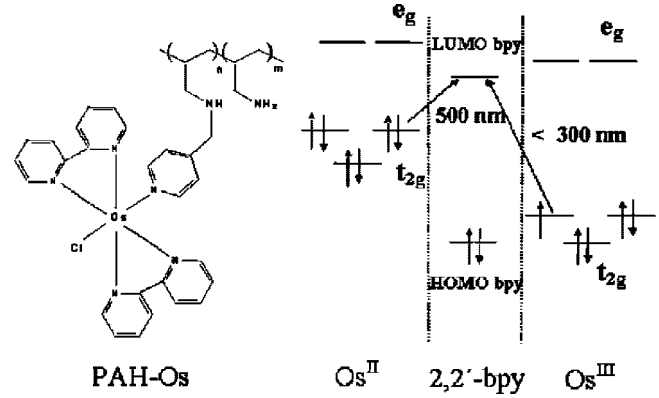

with H_2O_2 even in the presence of Au nanoparticles; however, the oxidation of Os(II) to Os(III) takes place in the presence of soybean peroxidase (SBP). Thus, to obtain the oxidized nanoparticles, Os(II) in the shell was oxidized by treatment with H_2O_2 catalyzed by soluble soybean peroxidase (SBP) followed by thorough washing and centrifugation steps as described in the experimental section. A careful study of the ζ potential of the resulting nanoparticles (see Supporting Information) indicates that negatively charged SBP remains adsorbed on the positively charged PAH-Os-covered nanoparticles even after several washing cycles.

Figure 6a (as grown) shows Raman spectra collected with 514.5 nm excitation from 1 μL drops of the core−shell NPs solution on atomically flat Au coated glass substrate (robax, Arandee, Germany) and prepared (i) as grown, that is, in its reduced Os(II) state, (ii) oxidized to Os(III), and (iii) reduced with glucose added to the oxidized sensor nanoparticles. In the oxidized state, Os(III), the Raman scattering spectrum of the nanoparticles vanishes almost completely (labeled "Oxidized" in Figure 6a). However, when 5 μL of 1 M glucose solution were added to 25 μL of solution of the oxidized nanoparticles, with a washing cycle of 35 min at 7000 rpm (4.500g) to remove excess glucose, the resonant Raman spectrum of 1 μL of solution

Scheme 2. Schematic Representation of Resonant Raman Interrogation of the Os(II) Concentration in Core−Shell Au NPs and Glucose Detection

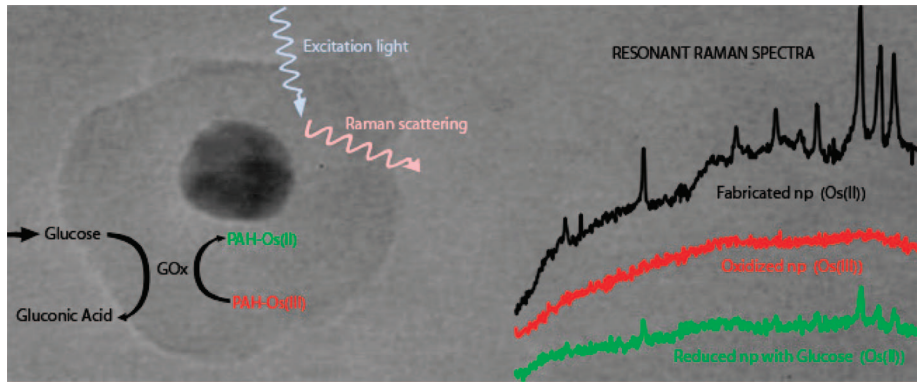

drop-deposited on flat Au shown in Figure 6a (labeled "Reduced with glucose") recovered to 20% of the original Os(II) NPs spectrum. Therefore, the recovery of the Os(II) resonant Raman intensity demonstrates the possibility of developing a photonic nanobiosensor using the core−shell nanoparticles.

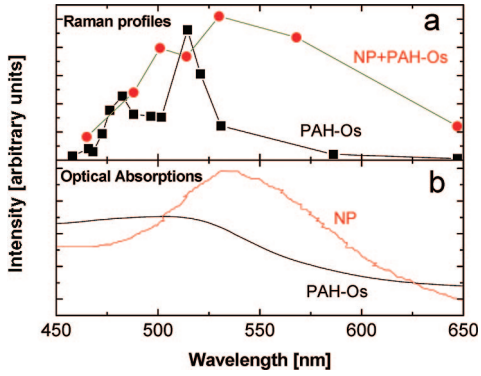

Figure 7. (a) Raman intensity of the 1550 cm^{-1} peak for the osmium complex bipyridine mode in PAH-Os as a function of the laser excitation energy both for the complex assembled in a layer-by-layer grown supramolecular structure of $(PAH\text{-}Os/PVS)_n$ ($n = 7$) grown on a glass substrate (i.e., without SERS effect) and in the core−shell nanosensor. (b) Detail of the absorption spectra of the PAH-Os complex in the region of the metal-to-ligand charge transfer (MLCT) transition and of the used Au-NPs. Note the close correspondence of the absorption maxima of the Os complex and the NPs, with the resonant Raman maxima for the pure complex and the core−shell sensors, respectively, thus demonstrating the role of SERS enhancement in the latter.

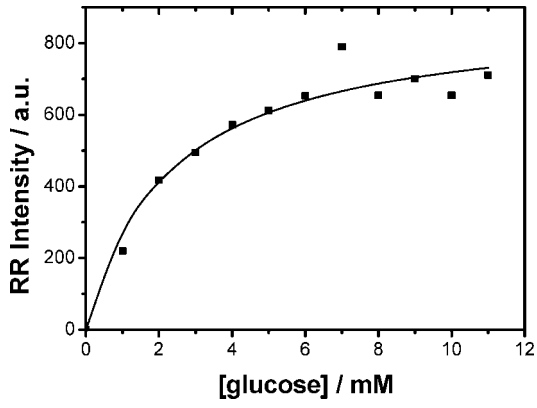

Figure 8. Resonant Raman scattering intensity vs glucose concentration in 1 μL of aqueous solution of 60 pM Au core $(PAH\text{-}Os)_4(GOx)_3$ shell nanoparticles on 700 nm Ag cavities. Excitation = 514.5 nm, 4.5 mW, two collections of 10 s for the vibration mode at 1480 cm^{-1}.

As discussed above, the spectra shown in Figure 6a are simultaneously enhanced by electronic and plasmon resonance effects, an amplification property that is intrinsic to the proposed nanosensor. It should be noticed however that, in this series of experiments where a 1 μL drop of the NPs solution was placed on a flat Au surface under the laser spot, no surface Raman enhancement is expected due to the gold surface.

On the other hand, the contact of the core−shell sensors with glucose can be sensed ex-situ exploiting the additional resonant enhancement of appropriately designed SERS substrates.[46] To illustrate this we show in Figure 6b spectra collected with the same sequence of samples (i−iii) presented in Figure 6a, but now with the Au core self-assembled multilayer shell nanoparticles deposited on a Ag close-packed hexagonal array of uniform spherical segment voids obtained by templated electrodeposited Ag thin films.[47] Bartlett et al. have shown strong surface enhanced Raman scattering for molecules adsorbed at these nanostructured surfaces[48,49] due to enhanced Raman scattering from surface plasmonic modes in the nanocavity array structure that couple to the excitation light.[50,51] While the resonant Raman scattering spectral features are apparent when the NPs are deposited on a flat Au surface (Figure 6a), a 500-fold enhancement of the signal is obtained when using the Ag-nanostructured cavity surface with a much better signal-to-noise ratio. The overall sensor response (i.e., oxidized vs reduced Os signal, and recovery after contact with glucose), however, remains unaltered, furthermore confirming its potentiality for analytical applications.

C. Glucose Concentration Dependence. We further investigated the glucose concentration dependence of the Raman signal as seen in a typical calibration curve (Figure 8) for the nanobiosensor where each point was measured with a fresh solution of nanoparticles and glucose, keeping the concentration of NPs constant (60.5 pM) while varying the glucose concentration. A 1 μL drop of solution containing the NPs and glucose was placed on a nanostructured Ag surface, and the Raman

(46) Abdelsalam, M.; Bartlett, P. N.; Russell, A. E.; Baumberg, J. J.; Calvo, E. J.; Tognalli, N.; Fainstein, A. *Langmuir* **2008**, *24*, 7018–7023.
(47) Abdelsalam, M. E.; Bartlett, P. N.; Baumberg, J. J.; Coyle, S. *Adv. Mater.* **2004**, *16*, 90.
(48) Abdelsalam, M. E.; Bartlett, P. N.; Baumberg, J. J.; Cintra, S.; Kelf, T.; Russell, A. E. *Electrochem. Commun.* **2005**, *7*, 740–744.
(49) Prakash, G. V.; Besombes, L.; Kelf, T.; Baumberg, J. J.; Bartlett, P. N.; Abdelsalam, M. E. *Opt. Lett.* **2004**, *29*, 1500–1502.
(50) Baumberg, J. J.; Kelf, T. A.; Sugawara, Y.; Cintra, S.; Abd∂elsalam, M. E.; Bartlett, P. N.; Russell, A. E. *Nano Lett.* **2005**, *5*, 2262–2267.
(51) Cole, R. M.; Baumberg, J. J.; Garcia de Abajo, F. J.; Mahajan, S.; Abdelsalam, M. E.; Bartlett, P. N. *Nanoletters* **2007**, *7*, 2094–2100.

scattering was measured exciting at 514 nm. After subtracting the background signal of the Os(III) NPs solution in the absence of glucose, the resonant Raman scattering intensity (1480 cm^{-1} mode) was plotted as a function of the glucose concentration. Figure 8 shows that the Raman intensity increases with the amount of glucose, reaching saturation at 7−8 mM glucose. Good fit of the experimental data to a Michaelis−Menten type equation is observed:

$$I = \frac{I_{max}}{1 + \frac{K_{app}}{[\text{glucose}]}} \quad (1)$$

(solid line in Figure 8), where I and I_{max} are the Raman intensity and the saturation value respectively and $K_{app} = 2.3$ mM is an apparent Michaelis−Menten constant for the ping-pong two-substrate glucose oxidase enzyme under those conditions.[52]

The results shown in Figure 8 indicate that the resonant Raman scattering intensity grows with the glucose concentration following the rate of glucose enzymatic oxidation and therefore the rate of Os(II) formation.

In the NPs shell we can estimate the osmium volume concentration in the submillimolar range by analogy to the concentration in similar LbL multilayers of glucose oxidase and PAH-Os on flat Au surfaces.[34] This is much less than glucose in all the solutions tested, which is in excess and should reduce completely all the Os(III) in the NPs present in the sample, resulting in a titration of the Os(III) by glucose and in a constant Raman signal for all glucose concentrations so a titration mechanism should be ruled out.

As an alternative explanation, it is suggested that the response curve shown in Figure 8 is given by a steady state Os(II) concentration that results from the competition of the enzymatic reduction of Os(III) by glucose and the reoxidation of the enzyme $FADH_2$ by molecular oxygen. The bimolecular rate for the reoxidation of $FADH_2$ in glucose oxidase by molecular oxygen is 1.8×10^6 M^{-1} s^{-1} at 25 °C[53] and since dissolved oxygen would equilibrate with the atmosphere in the sample microdrop, the reduction rate of Os(III) would vary with the concentration of glucose in the sample. Therefore, the rate of glucose enzymatic oxidation, which follows a Michaelis−Menten mechanism, would determine the concentration of the resonant Raman active Os(II) in the analyte sample:

$$\frac{[\text{Os(II)}]}{[\text{Os(III)}]} \propto \frac{\text{rate glucose}}{\text{rate oxygen}} \quad (2)$$

Since the oxygen concentration and thus the rate of its reduction is fairly constant, and [Os(tot)] = [Os(II)] + [Os(III)] in NP shell, the Raman intensity would be proportional to the Michaelis−Menten rate of the enzymatic glucose oxidation:

$$\text{Raman intensity} \propto \frac{\text{rate glucose}}{\text{rate glucose} + \text{rate oxygen}} \quad (3)$$

In the Supporting Information we show evidence that hydrogen peroxide (formed by reaction of traces of molecular oxygen with glucose oxidase $FADH_2$), cannot oxidize Os(II) directly or by redox catalysis in the presence of nanoparticles. However, with soybean peroxidase (SBP) adsorbed on the core−shell nanoparticles the oxidation of Os(II) by peroxide proceeds, which is consisistent with the mechanism described previously and in eq 3.

Conclusions

We have designed, as a proof of concept, a nanobiosensor based on a wired enzyme in the shell of Au core−shell nanoparticles with response to millimolar glucose concentration in solution. The nanobiosensor can be interrogated both (i) electrochemically as an amperometric enzyme electrode with the nanoparticles assembled on an electrode surface under potential control; or (ii) as a remote contactless photonic biosensor through the signal recovery of the Os(II) resonant Raman scattering intensity from a 1 μL sample volume with the nanoparticles both on atomically flat Au and on nanostructured Ag cavity arrays to further enhance the signal. The response to glucose concentration is based on the different resonant Raman behavior of the Os(II) and Os(III) polymer molecular wire.

It should be emphasized that all the components for the selective molecular recognition of the enzyme substrate and the generation of an electrical or an optical signal, the osmium molecular wire, and the glucose oxidase, are self-contained in each nanoparticle biosensor.

Acknowledgment. The authors are grateful to CONICET, University of Buenos Aires, and CNEA for financial support. ANPCyT (BID 1728 OC-AR PICT 2003 No. 06-17170) and the Argentine Nanotechnology Network PAV 2004 Project 22711- BID 1728/OC-AR grants are acknowledged. P.D.S. acknowledges a research doctoral fellowship from CONICET. E.J.C., H.T., and A.F. are permanent fellows of CONICET, Argentina. We thank Prof. Phil Bartlett for a short stay of N. Tognalli at Southampton to learn the template nanostructure techniques under Welcome Trust, U.K. (Grant 69713). Fruitful discussions on the biosensor mechanisms with M. Tagliazucchi are also gratefully acknowledged.

Supporting Information Available: Concentration of osmium and nanoparticles, oxidation of Os(III) contained in the nanoparticles, and transmission electron microscopy evidence. This material is available free of charge via the Internet at http://pubs.acs.org.

JA802318F

(52) Bartlett, P. N.; Toh, C. S.; Calvo, E. J.; Flexer, V. *Bioelectrochemistry* **2008**,
(53) Gibson, Q. H.; Swoboda, B. E. P.; Massey, V. *J. Biol. Chem. Lett.* **1964**, *239*, 3927–3934.